

Synthesis and Characterization of Air-Stable Elemental Fe Thin Films by Chemical Vapor Deposition of $\text{Fe}_3(\text{CO})_{12}$

On Mero, Nava Shpaisman, Judith Grinblat, Shlomo Margel*

Institute of Nanotechnology and Advanced Materials, Department of Chemistry, Bar-Ilan University, Ramat-Gan, Israel.
Email: *shlomo.margel@mail.biu.ac.il

Received May 7th, 2013; revised June 7th, 2013; accepted June 29th, 2013

Copyright © 2013 On Mero *et al.* This is an open access article distributed under the Creative Commons Attribution License, which permits unrestricted use, distribution, and reproduction in any medium, provided the original work is properly cited.

ABSTRACT

New magnetic air-stable nanogranular Fe thin films of 10 ± 1.2 nm thickness were prepared onto silicon wafers at 150°C under inert atmosphere by controlled Chemical Vapor Deposition (CVD) of triiron dodecacarbonyl ($\text{Fe}_3(\text{CO})_{12}$). These thin films, composed of sintered elemental Fe nanoparticles of 4.1 ± 0.7 nm diameter, are protected from air oxidation by a very thin carbon layer. The saturation magnetization of these thin Fe coatings was found to be close to that of bulk iron. The electrical resistivity behavior of the ferromagnetic thin films is similar to that of a semiconductor. In the present manuscript, these Fe thin coatings on Si wafers have been used as a catalyst for synthesizing crystalline carbon nanotubes (CNTs), by CVD using ethylene as a carbon precursor.

Keywords: Magnetic Conductive Thin Coatings; Thin Fe Films; Nanogranular Magnetic Thin Films; Magnetic Coatings; $\text{Fe}_3(\text{CO})_{12}$; CNTs

1. Introduction

Chemical Vapor Deposition (CVD) is a common technique for synthesizing thin coatings. This technique is based on the deposition of vapor of a desired material as thin films on a substrate surface. The process is usually performed in a controlled atmosphere (CVD) to avoid the interaction between the vapor and air [1,2]. In CVD, the material to be deposited is introduced as a precursor gas and then, still in the vapor phase, conformally coats the substrate surface [3,4].

Nanogranular magnetic films are composed of magnetic nanoparticles embedded in a non-magnetic isolating matrix such as SiO_2 , Si_3N_4 , Al_2O_3 , BN, C, etc. [5,6]. These magnetic films exhibit improved properties such as oxidation resistance, corrosion resistance and wear resistance. Elemental iron is the most useful ferromagnetic element for electromagnetic interference and radio frequency interference magnetic shielding applications. It is significantly cheaper than other ferromagnetic materials, it has the highest magnetic moment at room temperature, a high Curie temperature and a fairly low coercivity [7,8]. In addition, iron is a commonly available element, and therefore significantly cheaper than other ferromagnetic materials. Fe thin films are easily oxidized

by air and therefore significantly lose their high magnetic moment. To prevent these phenomena, previous publications already illustrated that the elemental Fe should be protected by a passivation layer such as carbon [9], silica [10], and alumina [11].

Thin films of transition metals are often used for the synthesis of carbon nanotubes (CNTs) [12]. In addition to their very high aspect ratio, their potential for chemical functionalization, and their characteristic electrical, mechanical, and thermal properties, CNTs have many applications including electronic devices (e.g., CNTs-based field effect transistors, interconnects for microprocessors, etc.), [13] electrodes for batteries [14,15] and supercapacitors [16], reinforced composites [17], etc. [18,19]. Typical catalysts widely employed in CNTs synthesis include transition metals, and more often ferromagnetic metals such as Co, Fe and Ni [20,21].

In the present study, the synthesis and characterization of new nanogranular Fe/C magnetic conductive thin coatings on Si wafers, by CVD of $\text{Fe}_3(\text{CO})_{12}$ at low temperature under inert atmosphere, are described. These films are composed of sintered elemental Fe nanoparticles protected from air oxidation by a very thin layer of carbon. Since the carbon concentration in these coatings is relatively low (<3%), we will refer to these coatings as “Fe coatings”. The potential use of these Fe coatings as cata-

*Corresponding author.

lysts for synthesizing CNTs has also been demonstrated.

2. Experimental Section

2.1. Materials

The following substrates and analytical-grade chemicals were purchased from a commercial source and were used without further purification: cover glass slides, ethanol and $\text{Fe}_3(\text{CO})_{12}$ protected by 1% - 10% methyl alcohol from Aldrich (Israel); P type, boron doped Si wafers with <100> orientation from Si-Mat, Israel; Ultra-high purity precursor gases (99.99999): ethylene, nitrogen, argon, hydrogen and a mixture of argon with 1% oxygen (Ar-O_2) were purchased from Maxima Air Separation Center Ltd., Israel. Alumina (Al_2O_3)-coated Si wafers were prepared at the Hebrew University, Jerusalem, Israel, by e-beam evaporation of 10 nm interlayer of alumina on Si wafers. Water was purified by passing deionized water through an Elga stat Spectrum reverse osmosis system (Elga Ltd., High Wycombe, UK).

2.2. Fabrication of the Nanogranular Fe Thin Films

Si wafers were cut into $7 \times 7 \text{ mm}^2$ samples, cleaned by sequential soaking in baths of ethanol, distilled water and again ethanol, and then dried with an N_2 gas flow. The thin film fabrication system is composed of a 90 cm long quartz tube furnace with an inside diameter of 35 mm and a 10 cm heating zone sealed by two glass connectors (one in each side of the quartz tube) which allow a gas flow of the inert gas from the gas canister. A brass crucible with three 7 mm^3 wells was positioned under the heating zone in the middle of the quartz tube. Prior to the thin film fabrication, 0.00317 mmol of $\text{Fe}_3(\text{CO})_{12}$ precursor was added to the bottom of each of the three 7 mm^3 wells in the crucible, and three 7 mm^2 Si wafers or carbon coated copper grids (TEM grids) were placed horizontally at the top of the wells. The crucible was then pushed into the middle of the quartz tube and kept under Ar atmosphere in the tube furnace. The temperature of the quartz tube was then raised to 150°C at a rate of $10^\circ\text{C}/\text{min}$ and then maintained at 150°C for 1 min. The precursor vapors were deposited on the heated (150°C) substrates and decomposed to produce the Fe thin films of $10 \pm 1.2 \text{ nm}$ thickness on the substrates.

Synthesis of the Fe thin films for the XRD measurements were performed similarly, substituting the Si wafers for glass wafers, Synthesis of the Fe thin films for the electrical resistance measurements and for the CNTs growth were performed similarly, substituting the Si wafers for alumina-coated Si wafers [22].

2.3. Fabrication of the CNTs

CNTs were grown on the Fe films by a CVD process

with ethylene as a precursor gas, according to the literature [23]. Briefly, the CVD system used was composed of two one-zone tube furnaces (Lindberg Blue) with a quartz tube with external diameter of 25 mm and MKS mass flow controllers. The Fe-alumina coated Si wafers were placed in a crucible in the heating zone at the bottom of the quartz tube. The preheating temperature in the first furnace was set at 770°C and the growth temperature in the second furnace was set at 750°C . The process consisted of a 15-min annealing step with flows of Ar (100 [sccm]) and H_2 (400 [sccm]) followed by 15-minute growth step with the additional flows of Ar-O_2 (100 [sccm]) and C_2H_4 (200 [sccm]) [23]. At the end of the growth step, the Ar-O_2 and C_2H_4 flows were stopped, a min. later the H_2 flow was stopped, and after another min. the quartz tube was pushed out from the furnace and the sample was cooled down to room temperature under Ar flow.

2.4. Characterization

The structure of the Fe thin films and the CNTs growth were investigated by High Resolution Transmission Electron Microscope, HRTEM, (JEOL JEM-2100 (LaB₆) at 200 kV). The HRTEM is integrated with a digital Scanning device (STEM) comprising of annular Dark-Field (DF) and Bright-Field (BF) detectors and a Thermo Scientific energy-dispersive X-ray spectrometer (EDS) system for elemental analysis. TEM observations were made by taking BF images, HRTEM images and selected area electron diffraction (SAED) patterns. Fourier Transform Analysis (FFT) of high resolution images technique was used for structural analysis of the Fe thin films. Scanning and mapping were performed in STEM mode and the elemental analysis was performed using the EDS system equipped with the Noran System Six software.

Specimens for observation in the HRTEM were prepared in three ways: 1) TEM lamella samples of the Fe thin films on Si wafers were fabricated through the Focused Ion Beam (FIB) FEI Helios 600 system. In this process, the region of interest is first covered with Pt to protect the Fe thin coatings from damage caused by the FIB milling process. Then, several adjacent holes of the film were milled by a gallium ion beam. Subsequently the lamella was lifted-up by a micromanipulator and glued on the TEM grid where the final thinning takes place; 2) Direct deposition of the Fe films on a standard carbon TEM support; 3) Scraping CNTs from the alumina-coated Si wafers into isopropanol and then putting one drop on the carbon TEM grids for characterization.

Surface elemental analysis was obtained by X-ray Photoelectron Spectroscopy (XPS; model AXIS-HS, Kratos Analytical, England) using Al $K\alpha$ lines, at 10⁻⁹Torr, with a take-off angle of 90° . Powder X-Ray Diffraction (XRD) patterns were recorded using an X-ray

diffractometer (model D8 Advance, Bruker AXS) with Cu K α radiation source filtered with a graphite monochromator ($\lambda = 1.5406 \text{ \AA}$). Measurements were performed at a temperature of 298 K, the X-ray beam was generated at 40 kV and 40 mA power and a 0.050° step-width with a 36 s counting time for each step where applied. Isothermal magnetization measurements at room temperature were performed in a commercial (Quantum Design) Superconducting Quantum Interference Device (SQUID) magnetometer. Mössbauer Spectroscopy (MS) studies were performed using a conventional constant acceleration drive and a 50 m Ci $^{57}\text{Co}:\text{Rh}$ source. The velocity calibration was performed at room temperature-Fe absorber, and the isomer shifts (I.S.). I.S. values reported are relative to that of iron. The observed spectra were least-square fitted by theoretical spectra, assuming a distribution of hyperfine interaction parameters, corresponding to non-equivalent iron locations differing in local environment. Electrical resistance characterization as function of temperature was performed in quantum design PPMS (Physical Property Measurement System). Four silver-paint contacts were used in all the electrical resistance measurements. The electrical resistance experiments were done by applying 5 μA current through the magnetic films; the temperature was raised at a rate of 6 K/min from 4 to 373 K. The samples were placed near to a standard Pt thermometer which monitored the temperature increase and measured voltage from a voltmeter was translated to the samples' electrical resistance.

3. Results and Discussion

HRTEM cross section image prepared by the FIB technique as described in the experimental part was used for characterization of the Fe thin films deposited on Si wafers. **Figure 1A** shows a typical Fe film image of $10 \pm 1.2 \text{ nm}$ thickness deposited on a Si wafer.

The Pt on top of the film is due to the FIB lamella preparation process as described in the experimental part. **Figure 1B** is the high-resolution image of the Fe nanoparticles that make up the Fe film (taken from an area of **Figure 1A**). It is clearly seen that this film is composed of a few layers of sintered Fe nanoparticles of $4.1 \pm 0.7 \text{ nm}$

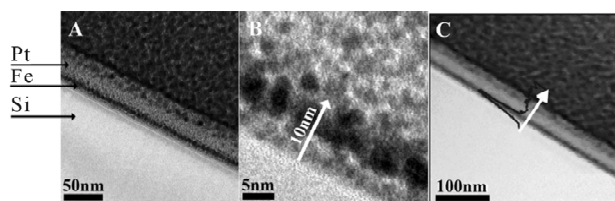


Figure 1. Cross-sectional TEM micrograph of a typical Fe thin film of $10 \pm 1.2 \text{ nm}$ thickness on a Si wafer (A). Image B is a HRTEM micrograph of image A and image C is a STEM image of the cross-section showing the iron's line scan in the blue curve.

diameter. **Figure 1C** illustrates STEM image of the line scan profile for the elemental Fe (blue). It is clearly shown that the peak in the blue curve is located at the same region as marked for Fe in images A and B.

A typical XRD pattern of these films, as shown in **Figure 2** exhibits peaks at $2\theta = 65.6^\circ$ (200) corresponding to the cubic bcc crystalline metallic Fe structure (MW = 55.85 g/mol, S.G: Im-3m, Z = 2, a = 2.86 \AA). The Fe composition and crystallinity of the Fe films were further investigated by Mössbauer Spectroscopy (MS). **Figure 3** presents the MS of a typical Fe thin film of $10 \pm 1.2 \text{ nm}$ thickness on a Si wafer. This figure shows typical sextets with hyperfine parameters.

The hyperfine parameters deduced for the major subspectrum (67%) are I.S. = 0 mm/s and $H_{\text{eff}} = 330 \text{ kOe}$. The distance between the two extreme peaks of the sextet is 10.5 mm/s, indicating pure metallic Fe. The thin film MS spectrum is composed of magnetically ordered and unordered nanoparticles; at room temperature, the sextet is associated with magnetically ordered (crystalline) particles (67%) while the main broad peak is associated with magnetically unordered (non-crystalline) particles (33%). Similar MS spectra were also observed for the other Fe coatings, regardless of their thickness.

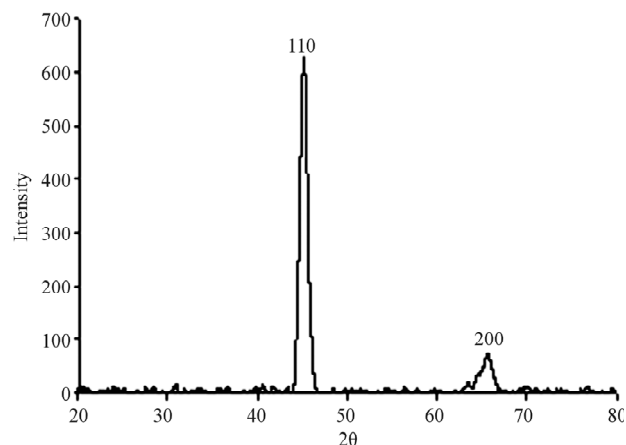


Figure 2. A typical XRD pattern of the Fe thin film.

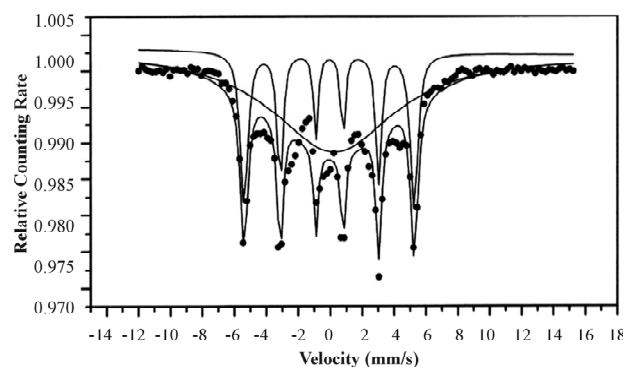


Figure 3. Mössbauer spectrum at room temperature of a typical Fe thin film on a Si wafer.

Table 1 lists the surface elemental composition of these Fe films as measured by XPS. These XPS measurements show that the films' surface is mostly composed of carbon (63.9% C, 6.5% Fe and 29.6% O), in contrast to their weight percent in the $\text{Fe}_3(\text{CO})_{12}$ precursor: 28.4% C, 37.8% O and 33.8% Fe. Overall, the XPS reflected electron beam decays as the x-ray beam penetrates deeper into the matter, hence the high surface concentration of C and low surface concentration of Fe together with the XRD results indicate that most of the carbon of the Fe films is concentrated in the outer layer of the magnetic film, thereby preventing the Fe content of the coatings from oxidizing in air. The surface content of O (29.6%) as shown in **Table 1** is probably related to oxidized Fe and C. High resolution XPS measurements, as shown in **Table 2**, indeed indicate that the carbon fraction of the most outer surface is composed of 76% C-C bonds and 24% of ether, carbonyl and carboxyl groups.

The magnetic properties of these Fe films coated on Si wafers were measured by the SQUID magnetometer at room temperature. **Figure 4** represents the field dependence of the magnetization measured at 300 K of a typical Fe coating of 10 ± 1.2 nm thickness on a Si wafer. This

Table 1. Surface elemental composition of a typical Fe thin film as measured by XPS.

Composition	Weight %		
	[Fe]	[C]	[O]
Surface	6.5	63.9	29.6

Table 2. Surface carbon functional groups analysis of a typical Fe thin film as measured by high resolution XPS.

Carbon bond type	Weight %			
	C-C	C-O	C=O	COO
Surface composition	76.0	4.5	9.1	10.4

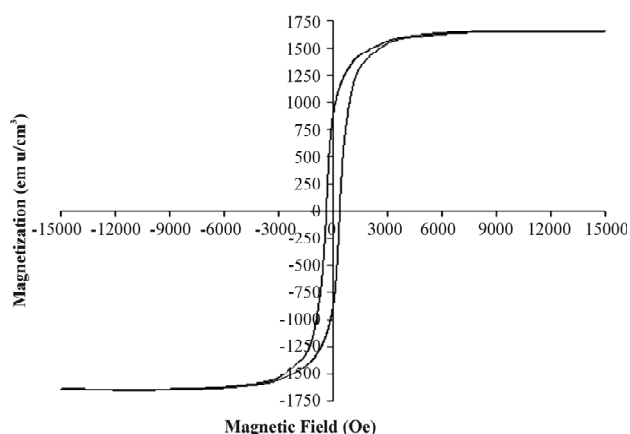


Figure 4. A magnetization curve of a typical Fe thin film.

figure shows a ferromagnetic-type curve as indicated by the existence of the hysteresis loop. The saturation magnetization (MS) and coercivity values obtained at 300 K were 1657 emu/cm^3 and 375 Oe. The MS bulk value of zero-valent Fe is 1734 emu/cm^3 while that of bulk magnetite is 480 emu/cm^3 [24,25]. The Ms value of this film is slightly lower than that of bulk elemental Fe probably due to the carbon and oxidized Fe existing on the surface of these films, as illustrated in **Table 1** by XPS measurements.

The nanostructure and composition of the Fe thin films were investigated by HRTEM microscopy. **Figure 5** presents a typical HRTEM photomicrograph of $2 \mu\text{m}^2$ area of a typical Fe thin film deposited on a carbon grid. The figure displays the well-resolved lattice-fringe contrast of the crystalline nanoparticles and their identification was based on the analysis of this high resolution image. Insert A (**Figure 5**) is the computed FFT of the portion of the image outlined by the white square. In this figure it is possible to identify unambiguously elemental Fe crystalline nanoparticles. This insert presents sets of reflections that can be assigned to the d 110 family of planes of the above mentioned Fe BCC structure. Insert B (**Figure 5**) demonstrates the filtered and magnified portion of the image outlined by the white square and shows the lattice fringes $d_{110} = 0.2 \text{ nm}$ of the cubic Fe BCC structure ($a = 2.86 \text{ \AA}$). Some clear and individual Fe nanoparticles displaying only the lattices of the d 110 plane can be discerned, as emphasized in the image, the existence of a non-crystalline matrix between nanoparticles defines them in **Figure 5**. HRTEM investigation of this film also revealed a very small and undefined portion of Fe_3O_4 phase, the distances measured between lattice fringes were 0.25 nm (d 222) and 0.26 nm (d 113) of the cubic

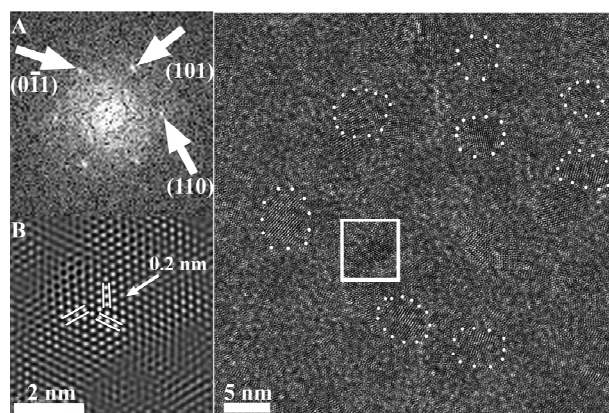


Figure 5. HRTEM of a $2 \mu\text{m}^2$ area of a typical Fe thin film deposited on a carbon grid. Insert A is the Fourier transform taken from the area marked by the white square showing sets of reflections matching the structure of elemental Fe. Insert B is the filtered and magnified image of the area marked by the white square, displaying the lattice fringes for elemental Fe.

Fe_3O_4 FCC structure ($a = 8.35 \text{ \AA}$), Utilization of these advanced nano-techniques, together with the XRD results provided unambiguous evidence that the thin films described in this study are composed of nanoparticles of elemental Fe (BCC structure unit cell parameter $a = 2.86 \text{ \AA}$). As the XRD measurements show only the presence of Fe, it can be concluded safely that the nano-regions of Fe_3O_4 found in these electron microscopy studies, are the result of bare Fe oxidation found on the most outer surface layer of the thin film when exposed to air.

Results showing that the films are composed mainly of elemental Fe have led us to the assumption that these films can be used as electric conductors. **Figure 6** demonstrates the electrical resistivity behavior of a typical Fe thin film as function of temperature ($I = 5 \mu\text{A}$) at a rate of 6 K/min from 4 to 373 K.

The measured electrical resistivity of the alumina-coated Si wafers before the Fe coating process was several $\text{K}\Omega$ s at all the measured temperatures. This result confirms that all resistivity results were not obtained from a substrate conduction leakage. **Figure 6** exhibits that the resistance of the Fe film decreased as the temperature increased, e.g., 1289 Ω at 38 K and 30 Ω at room temperature. This behavior resembles that of a semiconductor and can be correlated with the mixed crystalline and non-crystalline structure of the Fe films, which acts as an obstacle to electron flow at low temperatures [26]. Another interesting feature is observed at low temperatures wherein these $10 \pm 1.2 \text{ nm}$ thin films do not conduct in the region of $T \leq 37 \text{ K}$ ($R = \infty \Omega$). This phenomenon is probably related to the 2D structure of the $10 \pm 1.2 \text{ nm}$ film as shown in **Figure 1** [27,28]. This can be explained by the temperature-dependent evolution of the band gap and density of electron states in systems containing a low number of atoms such as two dimensional structures similarly to our thin film [29]. In 2-dimensional systems where nanocrystalline particles have distinct shapes and edges, the electron density of states is

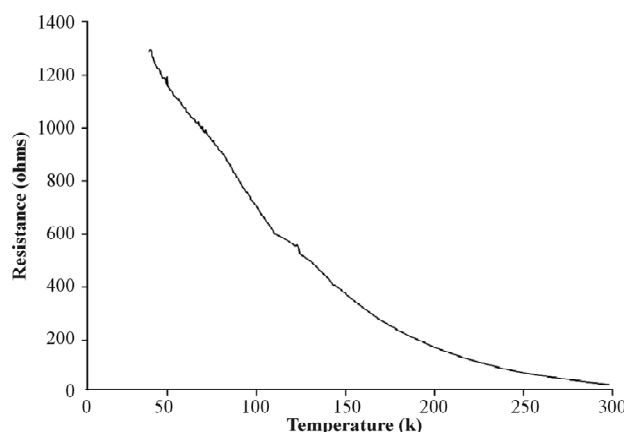


Figure 6. Electric resistance of a typical Fe thin film as a function of temperature.

localized below a critical energy (EC) also known as the “mobility edge”, separating localized and delocalized states. EC, in the $10 \pm 1.2 \text{ nm}$ Fe thin film, occurs at $T = 37 \text{ K}$, hence, below this temperature $R = \infty \Omega$, while above this temperature the electrons can overcome the non-crystalline, non-conducting matrix/nanoparticles and undergo tunneling between crystalline nanoparticles [26]. This result is also consistent with the Mössbauer result which showed 33% of non crystalline iron. This electric resistivity result in addition to the magnetization, XRD and Mössbauer measurements were repeated on the same films during 12 months and shown no significant change in the magnetic and electrical films properties. Typical catalysts widely employed in CNTs synthesis include transition metals, and often ferromagnetic metals such as Co, Fe and Ni [20,21]. Preliminary study indeed indicated that our Fe thin films can be used as precursors for synthesizing multi-wall CNTs (MWCNTs), as shown in **Figure 7**. The CNTs’ length was impossible to measure as they were not vertically aligned. The diameter, walls and length of the CNTs depend extensively on the film characteristics, the unique properties of the presented film and especially the condensed nanoparticle structure of the films.

4. Conclusion

This work demonstrates a simple CVD process for the fabrication of $10 \pm 1.2 \text{ nm}$ conductive magnetic Fe thin coatings on Si wafers. The films produced in this method show the metallic properties of the precursor’s metal and are composed of Fe nanoparticles condensed together and protected from oxidation by a very thin carbon layer. The preliminary potential use of these films as a catalyst for CNT growth has been illustrated. Further improvements of the Fe thin coating process, e.g., films of controlled thicknesses, and the formation of improved CNTs are planned for future investigation.

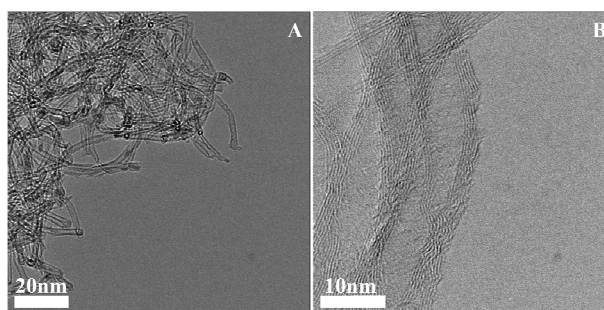


Figure 7. Typical HRTEM images of MWCNTs grown on the Fe thin coating on alumina-coated Si wafers. For the HRTEM pictures, the Fe coating containing the CNTs was scraped from the alumina-coated Si wafer and deposited onto the TEM carbon grid.

5. Acknowledgements

This study was partially supported by a Minerva grant (microscale and nanoscale articles and thin films for medical applications). We thank to Dr. Tomer Zimerin for helping in the preparation of the CNTs.

REFERENCES

- [1] I. Corrales-Mendoza, A. Conde-Gallardo and V. M. Sanchez-Resendiz, "Nd(1-x)Fe(x)O_F Thin Films Deposited by Chemical Vapor Deposition and Their Arsenic Diffusion," *IEEE Transactions on Applied Superconductivity*, Vol. 21, No. 3, 2011, pp. 2849-2852. [doi:10.1109/TASC.2010.2084983](https://doi.org/10.1109/TASC.2010.2084983)
- [2] M. L. Hitchman and K. F. Jensen, "Chemical Vapor Deposition, in: Principles and Applications," Academic Press, London, San Diego, 1993, p. 677.
- [3] Y. H. Low, M. F. Bain, D. C. S. Bien, J. H. Montgomery, B. M. Armstrong and H. S. Gamble, "Selective Deposition of CVD Iron on Silicon Dioxide and Tungsten," *Microelectronic Engineering*, Vol. 83, No. 11-12, 2006, pp. 2229-2233. [doi:10.1016/j.mee.2006.10.008](https://doi.org/10.1016/j.mee.2006.10.008)
- [4] Q. P. Wei, Z. M. Yu, M. N. R. Ashfold, Z. Chen, L. Wang and L. Ma, "Effects of Thickness and Cycle Parameters on Fretting Wear Behavior of CVD Diamond Coatings on Steel Substrates," *Surface & Coatings Technology*, Vol. 205, No. 1, 2010, pp. 158-167. [doi:10.1016/j.surfcoat.2010.06.026](https://doi.org/10.1016/j.surfcoat.2010.06.026)
- [5] Z. W. Liu and C. K. Ong, "Microstructure and Thickness Dependent Magnetic Properties of Nanogranular Co-Zn-O Thin Films For Microwave Applications," *Journal of Alloys and Compounds*, Vol. 509, No. 41, 2011, pp. 10075-10079. [doi:10.1016/j.jallcom.2011.08.039](https://doi.org/10.1016/j.jallcom.2011.08.039)
- [6] S. F. Zhang and P. M. Levy, "Conductivity and Magnetoresistance in Magnetic Granular Films," *Journal of Applied Physics*, Vol. 73, No. 10, 1993, pp. 5315-5319. [doi:10.1063/1.353766](https://doi.org/10.1063/1.353766)
- [7] F. S. Hung, F. Y. Hung and C. M. Chiang, "Crystallization and Annealing Effects of Sputtered tin Alloy Films on Electromagnetic Interference Shielding," *Applied Surface Science*, Vol. 257, No. 8, 2011, pp. 3733-3738. [doi:10.1016/j.apsusc.2010.11.126](https://doi.org/10.1016/j.apsusc.2010.11.126)
- [8] S. S. Azim, A. Satheesh, K. K. Ramu, S. Ramu and G. Venkatachari, "Studies on Graphite Based Conductive Paint Coatings," *Progress in Organic Coatings*, Vol. 55, No. 1, 2006, pp. 1-4. [doi:10.1016/j.porgcoat.2005.09.001](https://doi.org/10.1016/j.porgcoat.2005.09.001)
- [9] E. Sutter, p. Albrecht, F. E. Camino and P. Sutter, "Monolayer Graphene as Ultimate Chemical Passivation Layer for Arbitrarily Shaped Metal Surfaces," *Carbon*, Vol. 48, No. 15, 2010, pp. 4414-4420. [doi:10.1016/j.carbon.2010.07.058](https://doi.org/10.1016/j.carbon.2010.07.058)
- [10] Y. Wang, H. Gao, R. Yeredla, H. Xu and M. Albrecht, "Preparation of Iron Particles Coated with Silica," *Journal of Colloid and Interface Science*, Vol. 217, No. 1, 1999, pp. 203-207.
- [11] F. Jay, V. Gauthier and S. Dubois, "Iron Particles Coated with Alumina: Synthesis by a Mechanofusion Process and Study of the High-Temperature Oxidation Resistance," *Journal of the American Ceramic Society*, Vol. 89, No. 11, 2006, pp. 3522-3528.
- [12] M. Gaillard, C. Boulmer-leborgne, N. Semmar and E. Millon, A. Petit, "Carbon Nanotube Growth from Metallic Nanoparticles Deposited by Pulsed-Laser Deposition on Different Substrates," *Applied Surface Science*, Vol. 258, No. 23, 2012, p. 9237. [doi:10.1016/j.apsusc.2011.12.115](https://doi.org/10.1016/j.apsusc.2011.12.115)
- [13] P. Avouris, J. Appenzeller, R. Martel and S. J. Wind, "Carbon Nanotube Electronics," *Proceedings of the IEEE*, Vol. 91, No. 11, 2003, pp. 1772-1784. [doi:10.1109/JPROC.2003.818338](https://doi.org/10.1109/JPROC.2003.818338)
- [14] B. J. Landi, M. J. Ganter, C. D. Cress, R. A. DiLeo and R. P. Raffaele, "Carbon Nanotubes for Lithium Ion Batteries," *Energy & Environmental Science*, Vol. 2, No. 6, 2009, pp. 638-654. [doi:10.1039/b904116h](https://doi.org/10.1039/b904116h)
- [15] B. L. Ellis, K. T. Lee and L. F. Nazar, "Positive Electrode Materials for Li-Ion and Li-Batteries," *Chemistry of Materials*, Vol. 22, No. 3, 2010, pp. 691-714. [doi:10.1021/cm902696j](https://doi.org/10.1021/cm902696j)
- [16] M. Inagaki, H. Konno and O. Tanaike, "Carbon Materials for Electrochemical Capacitors," *Journal of Power Sources*, Vol. 195, No. 24, 2010, pp. 7880-7903. [doi:10.1016/j.jpowsour.2010.06.036](https://doi.org/10.1016/j.jpowsour.2010.06.036)
- [17] J. N. Coleman, U. Khan, W. J. Blau and Y. K. Gun'ko, "Small But Strong: A Review of the Mechanical Properties of Carbon Nanotube-Polymer Composites," *Carbon*, Vol. 44, No. 9, 2006, pp. 1624-1652. [doi:10.1016/j.carbon.2006.02.038](https://doi.org/10.1016/j.carbon.2006.02.038)
- [18] V. N. Popov, "Carbon Nanotubes: Properties and Application," *Materials Science & Engineering R-Reports*, Vol. 43, No. 3, 2004, pp. 61-102. [doi:10.1016/j.mser.2003.10.001](https://doi.org/10.1016/j.mser.2003.10.001)
- [19] M. Paradise and T. Goswami, "Carbon Nanotubes—Production and Industrial Applications," *Materials & Design*, Vol. 28, No. 5, 2007, pp. 1477-1489. [doi:10.1016/j.matdes.2006.03.008](https://doi.org/10.1016/j.matdes.2006.03.008)
- [20] A. M. Cassell, J. A. Raymakers, J. Kong, H. J. Dai, "Large Scale CVD Synthesis of Single-Walled Carbon Nanotubes," *Journal of Physical Chemistry B*, Vol. 103, No. 31, 1999, pp. 6484-6492. [doi:10.1021/jp990957s](https://doi.org/10.1021/jp990957s)
- [21] P. Chen, H. B. Zhang, G. D. Lin, Q. Hong and K. R. Tsai, "Growth of Carbon Nanotubes by Catalytic Decomposition of CH₄ or CO on a Ni-MgO Catalyst," *Carbon*, Vol. 35, No. 10-11, 1997, pp. 1495-1501. [doi:10.1016/S0008-6223\(97\)00100-0](https://doi.org/10.1016/S0008-6223(97)00100-0)
- [22] T. de los Arcos, F. Vonau, M. G. Garnier, V. Thommen, H. G. Boyen, P. Oelhafen, M. Duggelin, D. Mathis and R. Guggenheim, "Influence of Iron-Silicon Interaction on the Growth of Carbon Nanotubes Produced by Chemical Vapor Deposition," *Applied Physics Letters*, Vol. 80, No. 13, 2002, pp. 2383-2385. [doi:10.1063/1.1465529](https://doi.org/10.1063/1.1465529)
- [23] G. D. Nessim, A. Al-Obeidi, H. Grisar, E. S. Polsen, C. R. Oliver, T. Zimrin, A. J. Hart, D. Aurbach and C. V. Thompson, "Synthesis of Tall Carpets of Vertically Aligned Carbon Nanotubes by *In-Situ* Generation Of Water Vapor through Preheating of Added Oxygen," *Carbon*,

Vol. 50, No. 11, 2012, pp. 4002-4009.

[doi:10.1016/j.carbon.2012.04.043](https://doi.org/10.1016/j.carbon.2012.04.043)

- [24] R. M. Bozorth, "Ferromagnetism (Chapter XII)," D. Van Nostrand Company, New York, 1951.
- [25] Q. W. Chen, Y. T. Qian, Z. Y. Chen, Y. Xie, G. E. Zhou and Y. H. Zhang, "Hydrothermal Deposition of Magnetite (Fe₃O₄) Thin-Films," *Materials Letters*, Vol. 24, No. 1-3, 1995, pp. 85-87. [doi:10.1016/0167-577X\(95\)00081-X](https://doi.org/10.1016/0167-577X(95)00081-X)
- [26] Y. Qi, K. Sakai and H. Murakami, "Thickness Effect on Sheet Resistance in BSCCO Mixed Crystal Thin Film," *Journal of Low Temperature Physics*, Vol. 117, No. 3-4, 1999, pp. 669-673.
- [27] A. Kanda, S. Katsumoto and S. Kobayashi, "Charge-Soliton Transport-Properties in 2-Dimensional Array of Small Josephson-Junctions," *Journal of the Physical Society of Japan*, Vol. 63, No. 12, 1994, pp. 4306-4309. [doi:10.1143/JPSJ.63.4306](https://doi.org/10.1143/JPSJ.63.4306)
- [28] J. Siegel, O. Lyutakov, V. Rybka, Z. Kolska and V. Svorcik, "Properties of Gold Nanostructures Sputtered on Glass," *Nanoscale Research Letters*, Vol. 6, 2011, p. 96. [doi:10.1186/1556-276X-6-96](https://doi.org/10.1186/1556-276X-6-96)
- [29] G. D. Nessim, "Carbon Nanotube Synthesis with Special Focus on Thermal Chemical Vapor Deposition," *Nanoscale*, Vol. 2, No. 8, 2010, pp. 1306-1323. [doi:10.1039/b9nr00427k](https://doi.org/10.1039/b9nr00427k)